Research on the Spectral Variation of the Black Hole X-ray Binaries with the Monte Carlo Simulation

Zhengyang Zhang
Chadwick School, Palos Verdes Peninsula, USA
zzhang2027@chadwickschool.org

Abstract. This study investigates the spectral variation of black hole X-ray binaries using Monte Carlo Simulations for different spatial distributions of cold gas clouds in hot accretion flows. The variation of inhomogeneous accretion flow can be described with different physical parameters, including temperature gradients, optical depth, cloud coverage, and reflection efficiency. The results indicate that higher optical depth enhances photon scattering, significantly increasing the cooling rate and producing denser cold cloud distributions. Systems with temperature gradients exhibit higher cooling rates in the inner regions, where hot gas transitions into cold clouds more efficiently. Additionally, greater cloud coverage and reflection efficiency lead to widespread and uniform cold cloud formation across larger areas. The findings demonstrate that both local physical conditions and global cloud configurations play crucial roles in the state transition process of black hole X-ray binaries.

Keywords: Monte Carlo Simulations, Black Hole, X-ray binaries, cold cloud formation.

1. Introduction

1.1. Background on Black Hole X-ray Binaries

Black Hole X-ray Binaries (BHXBs)—systems where a black hole accretes material from a companion star—are some of the most intriguing objects in astrophysics. As materials are captured by the gravity of a black hole, they spiral toward the black hole and form an accretion disk by internal viscosity. This process makes BHXBs some of the brightest X-ray sources in the universe [1][2]

BHXBs are classified into low-mass X-ray binaries (LMXBs) or high-mass X-ray binaries (HMXBs), depending on the mass of the companion star [6]. For HMXBs, the stellar winds of the companion star are strong and keep providing fuel to the BH, and therefore, they are persistent X-ray sources. While for the LMXBs, the BH accretion occurs via Roche lobe Overflow, which means the source remains in quiescence or outbursts depending on whether the companion star fills its Roche lobe. Different X-ray states have been found during the outburst of LMXBs: the hard state (HS), the soft state (SS), and the intermediate state (IS).

1.2. X-ray States

The hard state is characterized by high-energy X-rays produced through Compton scattering in a hot, optically thin region close to the black hole. High-energy photons with a photon index less than 2 dominate the X-ray spectrum in the hard state. This harder spectrum arises mainly from Comptonization, where soft photons from the accretion disk scatter off hot electrons in the optically thin corona. In this state, the accretion disk is truncated at larger radii. The region near the black hole becomes filled with a hot, optically thin corona. Here, soft photons from the disk gain energy through repeated scattering by hot electrons, producing the harder X-rays observed [3] [4]

Conversely, the soft state is dominated by thermal X-rays emitted from a geometrically thin, optically thick accretion disk that extends close to the event horizon. Thermal emission from the optically thick, geometrically thin accretion disk dominates the soft state, with a photon index greater than 2. In this state, the Standard Accretion Disk (SAD) extends close to the black hole. It emits thermal radiation that effectively dissipates the energy of the infalling material.

The intermediate state lies between these extremes, combining features of both hard and soft states. Its spectrum reflects a mix of thermal emission from the disk and non-thermal Comptonization in the hot corona. During IS, the Standard Accretion Disk (SAD) moves inward toward the innermost stable circular orbit (ISCO) while the hot accretion flow recedes and adjusts.[5] This overlap creates a blend of thermal and non-thermal emissions, which vary depending on the energy distribution within the system. The intermediate state is also marked by hysteresis, where the luminosity required for transitions between states depends on the system's previous activity [7]. This phase raises key questions: How do changes in the accretion flow drive the observed spectral transitions? What physical processes govern the interplay between the corona's cooling and the SAD's extension toward the innermost stable circular orbit (ISCO)?

1.3. Research Objective and Methodology Overview

This research aims to find the processes that control these transitions by focusing on the intermediate state. This will help us understand how the system evolves between the hard and soft states, providing insights into the physics of accretion flows and radiation production under extreme gravitational conditions. In addition, we use Monte Carlo simulations to produce random numbers, as we can use them to simulate the interactions between protons and electrons and trace their paths through the accretion flow, which we can then collect and determine the physical process of the intermediate state.

2. Methodology

2.1. Simulation Overview

This study aims to determine the distribution of the radiative cooling rate and investigate how the density and distribution of cold clouds in the accretion disk influence it.

2.2. Photon Sampling

We simulate the transportation of a photon in four steps. First, we perform seed photon sampling to select the initial photons. Next, we assess whether the seed photon undergoes interaction with an electron. Then, we sample the interaction's position and the output photon's direction and energy. Finally, we repeat these three steps until the photon escapes. After tracing a large number of photons, the distribution of the cooling rate and the output spectrum can be obtained.

In the first step, the photon sampling, the distribution of luminosity for a Standard Accretion Disk (SAD) is used to determine the initial radial position of the seed photon since the probability density is proportional to the luminosity. When the radius is set, the temperature of the local disk can be derived from the SAD model. Since SAD emission is a blackbody, the frequency of a seed photon can be drawn by Planck's Law, which describes the spectral radiance of a blackbody at temperature T and frequency ν as follows,

$$B_\lambda(T) = \frac{8\pi h\nu^3}{c^3}\frac{1}{e^{\frac{h\nu}{k_B T}}-1},$$

where h is Planck's constant, ν is the frequency, c is the speed of light, and k_B is Boltzmann's constant. As for the direction of the seed photon, we assume it is isotropic over the disk surface.

2.3. Photon Interaction Probability

In the second step, we determine whether the seed photon interacts with an electron. Ignoring the emission of the hot gas, the radiation transfer can be described by the equation:

$$\frac{dI_\nu}{ds} = -k_\nu I_\nu,$$

where $k_\nu = n\sigma_\nu$ is the absorption coefficient, n is the number density of the seed photon, and I_ν is the specific intensity of the radiation. To find the intensity of the seed electron at a certain distance s, we integrate the function:

$$I_\nu(s) = I_\nu(s_0)exp\left[-\int_{s_0}^{s} k_\nu(s')ds'\right] = I_\nu^0 e^{-\int_0^s k_\nu ds} = I_\nu^0 e^{-\tau_\nu},$$

where s is the distance traveled and $\tau_\nu = \int_0^s k_\nu ds$ is the optical depth at a given frequency. The solution implies that the probability of the photon traveling a distance s without scattering is $e^{-\tau_\nu}$.

First, we calculate the optical depth, τ_ν, from the point where the seed photon is sampled to the surface of the accretion flow in one direction. Here, we assume the geometry and the properties, temperature, and density of the hot gas are locally homogeneous and axis-symmetric.

Next, we sample a random number ξ to compare with $e^{-\tau_\nu}$, the probability that the seed photon travels a certain distance without being absorbed or scattered. If $\xi > e^{-\tau_\nu}$, the photon is scattered; if $\xi < e^{-\tau_\nu}$, the photon escapes. If the photon is scattered, the free path that the photon traveled can be sampled by the probability density distribution $1 - e^{-\tau_\nu}$.

2.4. Scattering and Absorption Processes

In the third step, we determine the interaction's position and the emitting photon's direction and energy. As for the interaction, either scattering or absorption, we evaluate the corresponding cross-section. For scattering events, the cross-section σ_s is represented by the Klein-Nishina formula:

$$\sigma_s = 2\pi r_e^2\left\{\frac{1+\Gamma}{\Gamma^3}\left[\frac{2\Gamma(1+\Gamma)}{1+2\Gamma} - ln(1+2\Gamma)\right] + \frac{1}{2\Gamma}ln(1+2\Gamma) - \frac{1+3\Gamma}{(1+2\Gamma)^2}\right\},$$

where $\Gamma = \frac{h\nu_i}{m_e c^2}$, h is Planck's constant ($6.626 \times 10^{-34} Js$), ν_i is the frequency of the incident photon, m_e is the rest mass of the electron ($9.109 \times 10^{-31} kg$), and c is the speed of light in a vacuum ($3.00 \times 10^8\ m/s$). Similarly, we replace σ_s with σ_a in absorption events and calculate the result. The probability of scattering or absorption is determined by the following:

$$\text{if } \xi \le \frac{\sigma_s}{\sigma_s+\sigma_a}, scatter; \text{ if } \xi > \frac{\sigma_a}{\sigma_a+\sigma_s}, absorb.$$

In addition, the intensity of the seed photon along its path changes based on the properties of the medium. In scattering events, we assume the electrons are in thermal equilibrium, implying electron velocities follow the Maxwell-Boltzmann distribution:

$$f(E) \propto E^{\frac{1}{2}} e^{-\frac{E}{k_B T}}$$

where E is the kinetic energy of an electron, k_B is the Boltzmann constant, and T is the temperature of the hot gas or the cold disk (depending on the situation). Using this, we draw out the energy of the electron. Then, we use the Klein-Nishina formula to sample the energy and direction of the scattered photon, which is shown as follows:

$$\frac{d\sigma}{d\Omega} = \frac{1}{2} r_e^2 \left(\frac{\nu}{\nu_i}\right)^2 \left(\frac{\nu_i}{\nu} + \frac{\nu}{\nu_i} - sin^2\theta\right),$$

where ν_i is the frequency of the incident photon, ν is the frequency of the scattered photon, and θ is the scattering angle. For absorption events, we assume the gas is neutral and not ionized. Meanwhile, since each atom's absorption cross-section differs, we suppose the gas is solar-abundant. Since absorption cross-sections vary for different atoms, we also use the Klein-Nishina formula to calculate the energy and direction of absorbed photons.

2.5. Photon Tracking and Weighting

Additionally, since multiple scattering events are low-probability occurrences, we introduce a weighting factor to balance this in simulations. The program tracks the electron until its weight approaches zero, at which point the electron is ignored. The likelihood of scattering decreases exponentially, governed by $e^{-\tau_\nu}$.

3. Results

3.1. Same Temperature, Different Optical Depth

In figure 1 and 2, this simulation reveals that the cooling rate positively correlates with increasing optical depth. As the optical depth increases, more photons undergo scattering, resulting in more efficient cooling. The spatial distribution of cold clouds indicates that regions with higher optical depth contain denser and more localized cold clouds.

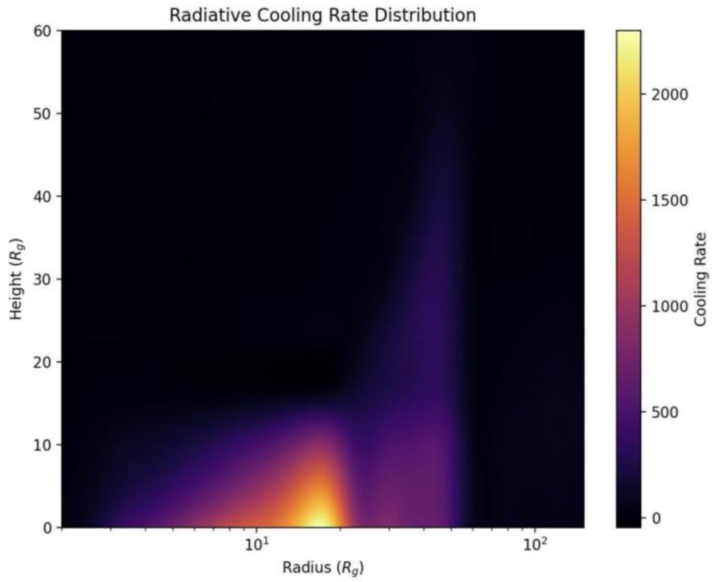

Figure 1. Cooling rate versus optical depth with cloud distribution visualization. Simulation parameters: temperature: $Tc(1) = Tc(2) = 100\ kEv$; optical depth:$\tau hc(1) = \tau hc(2) = 0.1$.

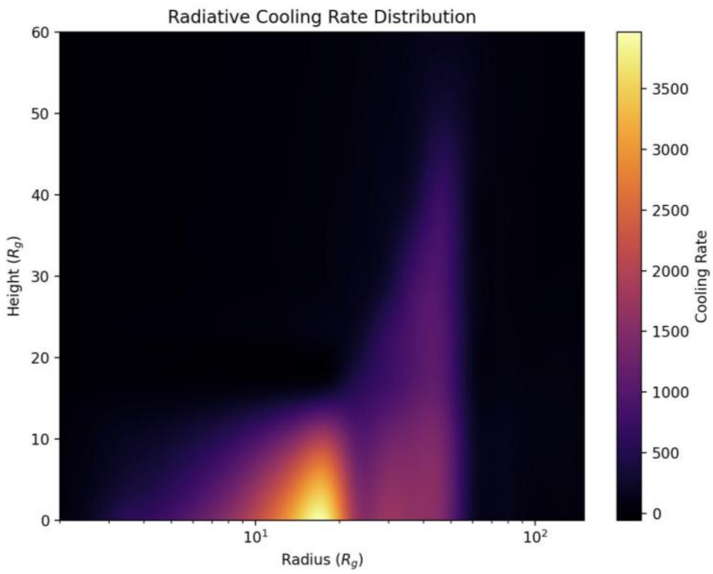

Figure 2. Cooling rate versus optical depth with cloud distribution visualization. Simulation parameters: temperature: $Tc(1) = Tc(2) = 100\ kEv$; optical depth: 5.

3.2. Temperature Gradient: High Inside, Low Outside

In figure 3, temperature gradients significantly impact the cooling rate within the accretion flow. This simulation, which incorporates higher temperatures in the inner regions and lower temperatures in the outer regions, produces the highest cooling rates near the black hole. The results demonstrate that cold clouds preferentially form near the black hole, where the temperature is raised. The outer regions show a gradual decrease in cloud density, which is consistent with the reduced cooling rate at lower temperatures.

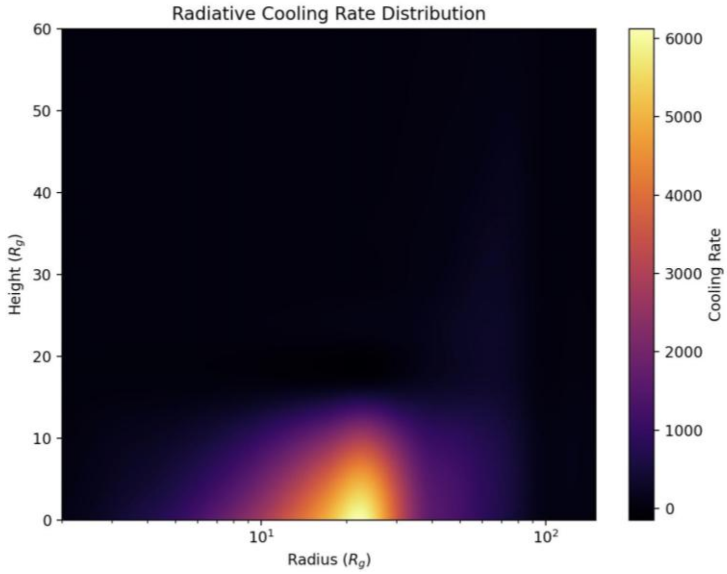

Figure 3. Cooling rate versus radial distance for temperature gradient simulation. Simulation parameters: temperature: $Tc(1) = 200\ kEv$, $Tc(2) = 100\ kEv$; optical depth: $\tau hc(1) = \tau hc(2) = 0.1$.

3.3. Higher Reflection and Radiation Efficiency

In figure 4, this simulation indicates that both reflection efficiency and cloud coverage enhance the cooling rate. A higher reflection rate increases the likelihood of photon scattering, while more significant cloud coverage facilitates more extensive cloud formation. Compared to other scenarios, the resulting spatial distribution of cold clouds is more uniform and extends further from the black hole.

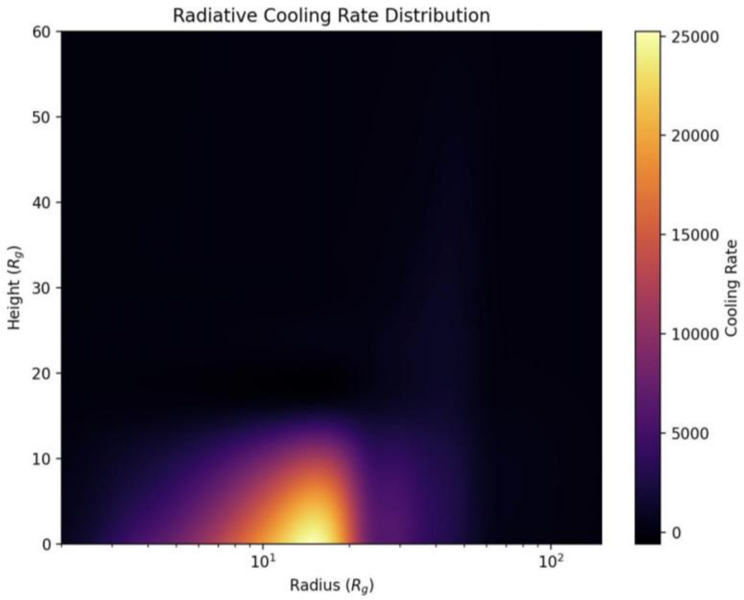

Figure 4. Cooling rate versus radial distance with high reflection rate and cloud coverage. Simulating parameters: temperature: $Tc(1) = 200\ kEv$, $Tc(2) = 100\ kEv$; fraction of reflection: albedo = 0.9; covering factor of the cold cloud for each cloud-gap unit: f_{cover} = 0.5; optical depth: $\tau hc(1) = \tau hc(2) = 0.1$.

3.4. Multi-Temperature Structure with High Optical Depth

In figure 5, this simulation involves multi-temperature structures with high optical depth and produces uniformly high cooling rates across the entire simulation domain. The combination of multiple temperature layers and elevated optical depth accelerates the formation of widespread cold clouds without sharp concentration in any particular region. This demonstrates the complexity of the intermediate state in black hole X-ray binaries, where thermal and non-thermal components coexist.

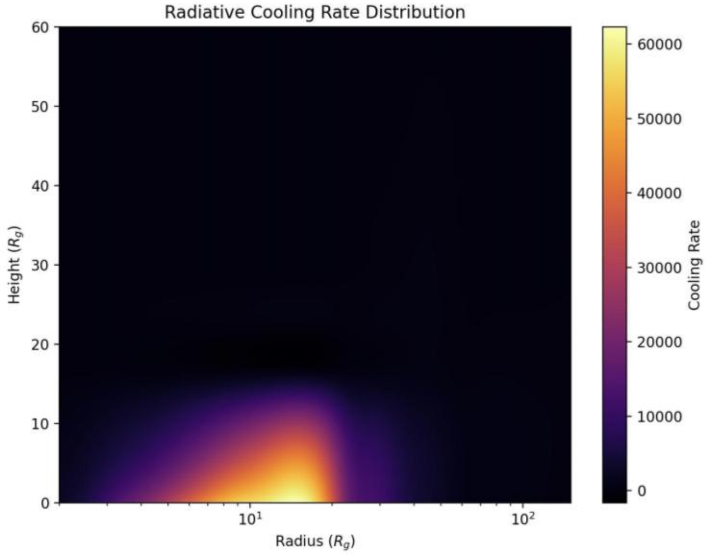

Figure 5. Cold cloud distribution for multi-temperature structure. Simulating parameters: temperature: $Tc(1) = 250\ kEv$, $Tc(2) = 150\ kEv$; optical depth: $\tau hc(1) = 0.8$, $\tau hc(2) = 0.5$; radius where cold disk becomes continuous: $r_{con} = 30.0$.

3.5. Larger Cloud Coverage and Reflection

Increasing the number of clouds and reflection efficiency results in higher cooling rates across more extensive spatial regions in figure 6. This configuration yields the most widespread cloud distribution observed in the simulations, with cold clouds covering significant portions of the accretion flow. This finding suggests that cloud coverage and reflection efficiency dominate the spatial structure of cold clouds within the accretion flow.

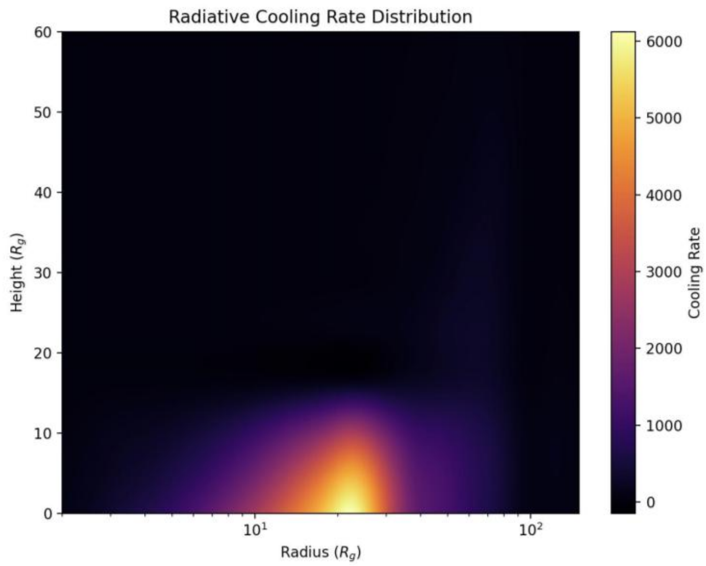

Figure 6. Cold cloud distribution with larger cloud coverage and reflection efficiency. Simulating parameters: number of cold clouds $n_{cl} = 5$; covering factor of the cold cloud for each cloud-gap unit: $f_{cover} = 0.5$; fraction of reflection: albedo = 0.9; temperature: $Tc(1) = 200\ kEv$, $Tc(2) = 100\ kEv$.

4. Conclusion

The results of this study demonstrate that the spectral variation of black hole X-ray binaries is linked to the distribution and formation of cold clouds within the accretion flow. The Monte Carlo simulations show that several interdependent physical parameters govern the cooling rate. Optical depth significantly influences the cooling process by enhancing photon scattering, which increases the probability of cold cloud formation in dense regions. Temperature gradients contribute to the spatial variation of cold clouds, with higher temperatures near the black hole promoting more efficient cooling in the inner regions. Reflection efficiency and cloud coverage further modify the spatial distribution, promoting the widespread formation of cold clouds across the accretion flow. Multi-temperature structures, combined with high optical depth, generate uniform cooling rates and cloud distributions, closely resembling the intermediate state of black hole X-ray binaries.

References

[1] Remillard, R. A., & McClintock, J. E. (2006). X-ray properties of black-hole binaries. Annual Review of Astronomy and Astrophysics, 44, 49–92.

[2] Shakura, N. I., & Sunyaev, R. A. (1973). Black holes in binary systems. Observational appearance. Astronomy and Astrophysics, 24, 337-355.

[3] Zdziarski, A. A., & Gierliński, M. (2004). Radiative processes, spectral states, and variability of black-hole binaries. Progress of Theoretical Physics Supplement, 155, 99-119.

[4] Yu, X.-D., Ma, R.-Y., Li, Y.-P., Zhang, H., & Fang, T.-T. (2018). The profiles of Fe K α line from the inhomogeneous accretion flow. Monthly Notices of the Royal Astronomical Society, 476(2), 2045-2052.

[5] Yuan, F., & Narayan, R. (2014). Hot accretion flows around black holes. *Annual Review of Astronomy and Astrophysics, 52*, 529–588. https://doi.org/10.1146/annurev-astro-082812-141003

[6] Hynes, R. I. (2010). Black hole binaries. New Astronomy Reviews, 54(7), 149-154.

[7] Yu, X.-D., Li, Y.-P., Xie, F.-G., & Ma, R.-Y. (2017). A Monte Carlo study of the spectra from inhomogeneous accretion flow. *Research in Astronomy and Astrophysics, 17*(8), 86. https://doi.org/10.1088/1674-4527/17/8/86